ACS Energy LETTERS

http://pubs.acs.org/journal/aelccp

LETTER

Accelerated Electrocatalyst Degradation Testing by Accurate and Robust Forecasting of Multidimensional Kinetic Model with Bayesian Data Assimilation

Miao Wang, Akimitsu Ishii, and Ken Sakaushi*

Cite This: ACS Energy Lett. 2025, 10, 22−29

Read Online

ACCESS | Metrics & More | Article Recommendations | Supporting Information

ABSTRACT: Degradation tests represent a significant bottleneck in electrochemical technology development, occasionally requiring tens of thousands of hours. Thus, reliable degradation forecasting in a short time frame is a game-changer in accelerating the establishment of future electrochemical devices. Herein, we show a multidimensional kinetic model for electrocatalyst degradation by quantifying the relationship among potential, current, and time, applicable under various conditions. Aiming to predict reliable degradation behaviors in shorter experimental timeframes and inspired by modern weather forecasting methods, we integrated Bayesian data assimilation with our model to expedite multidimensional parameter optimization. Consequently, we achieved accurate and robust forecasting of electrocatalyst lifetime by employing oxygen evolution reaction as a representative system: it takes just 300 h to obtain the final lifetime of close to 1000 h even with environmental noise. This data-driven approach can accelerate our understanding of the microscopic electrochemical mechanisms and simultaneously directly bridge this understanding to develop next-generation energy technologies.

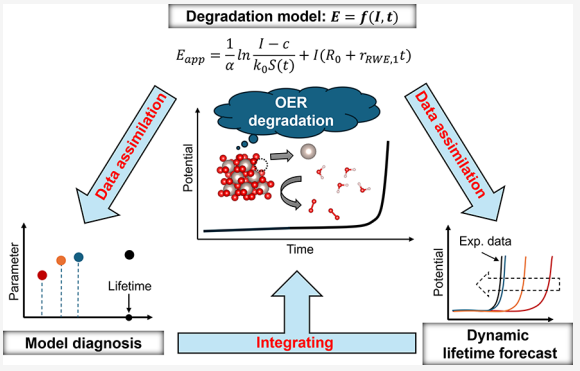

The accelerated implementation of next-generation electrochemical technologies is imperative for achieving carbon neutrality.[1,2] In particular, various types of electrolyzers are crucial for producing a wide spectrum of essential chemicals without carbon dioxide (CO_2) emissions. Although electrolysis is an old technology dating to the 18th century,[3] modern electrolyzer systems are key in the 21st century: in the present time, different cathodic reactions are combined with oxygen evolution reaction (OER) in an electrolyzer,[4] such as hydrogen evolution reaction in water/seawater splitting toward green hydrogen production,[5] CO_2 reduction reaction for high-value chemical production,[6,7] and nitrogen reduction reaction for green ammonia synthesis.[8−11] As such, electrolyzer technology is indispensable for the sustainable development of human societies in the 21st century,[4,12−14] which has triggered worldwide intensive research in affordable and sustainable yet high-performance electrocatalysts. For device implementation, electrocatalyst robustness is of great importance same as promoting the electrocatalytic activity to keep high overall energy efficiency during the operation time frame typically a decade or more.[5,15,16] To this end, one key relies on improving the durability of the OER electrode, i.e., the anode lifetime.[2,17−19] This is increasingly important because of the unclear fundamental understanding of related microscopic reaction mechanisms,[20−23] especially for the electrocatalyst degradation process.[24−26] Moreover, a durability evaluation for OER requires a long time, typically several thousand hours, and occasionally tens of thousands of hours.[2] Therefore, reliable methods to forecast anode lifetime in a short time frame are indispensable for accelerating the development of prospective electrolyzers.

Here we employ Bayesian data assimilation (DA) to obtain reliable interpretation of microscopic degradation mechanism

Received: October 16, 2024
Accepted: November 15, 2024

and estimation of model parameters for lifetime forecasting. DA, a data-driven method, features a combination of a well-defined simulation model and dynamic experimental data through effective algorithms, such as an ensemble Kalman filter or a four-dimensional variational method.[27,28] Consequently, DA has the ability to improve future forecast features and modeling simultaneously. Typical applications of DA can be found in modern meteorology and oceanography, and we are inspired by successful implementation of DA in these fields resulting, for instance, in quite accurate and robust weather forcasting.[29−31] Recently, aiming to see the potential of DA in electrochemistry, we employed an ensemble Kalman filter/smoother-based DA to understand microscopic mechanisms in electrochemistry.[32] As a result, we revealed a plausible relationship between the free energy of activation in the step of oxygen adsorption and the change of slope in the polarization curve of the oxygen reduction reaction, which could not be discovered by just a kinetic model. Hence, the DA method shows significant application potential in clarification of the electrode process;[33] this is a quite different from "black box" machine learning, which is somewhat unsatisfactory because of the problematic explanation of microscopic mechanisms.[34]

Based on the above considerations, after inspecting possible influences from the electrode−electrolyte interface on the performance of the OER, in this work, we established a practical theoretical model to forecast the degradation process of the OER electrocatalysts with a DA method based on the electrocatalyst dissolution process (Figure 1). As shown below, this DA-based method shows superior advantages over existing computational methods such as theoretical calculation based on molecular dynamics, machine learning methods, or typical fitting, as evidenced by quantitative comparison. Thus, this approach provides an alternative approach to drastically accelerate electrochemical degradation testing. The OER degradation model was built by focusing on dissolution of electrocatalysts with an energetic-span-model (ESM)-based kinetic analysis.[35−40] Through this degradation model, we achieved a dynamic forecast of the anode lifetime for the OER by iteratively conducting DAs with continuously updated experimental data. A model diagnosis was successfully conducted according to the DA results, and the key issues of the present model were clarified with guidance for future modification. The proposed degradation model and the coupling with data science in this study opens the way to durability exploration in oxygen electrocatalysis, which we believe will benefit widely practical applications of electrochemical techniques for renewable energies in the coming decades.

Considering electrochemical processes in the anode−electrolyte interface, we summarized possible effects on electrocatalyst degradation, including (1) dissolution of catalyst, (2) agglomeration, (3) detachment of catalyst, (4) blocking effect by adsorption/(re)deposition, (5) bubble blocking, (6) passivation, and (7) dissolution of substrate.[26,41,42] During the above effects, the loss of active site (mainly by dissolution) was noteworthy under strong anodic OER conditions[42−44] and thus was highlighted in this study (see more details in the discussion for Figure S1 in the Supporting Information (SI)). We described the OER activity according to the ESM-based kinetics[35−39] and finally obtained an equation set to quantify the degradation process toward

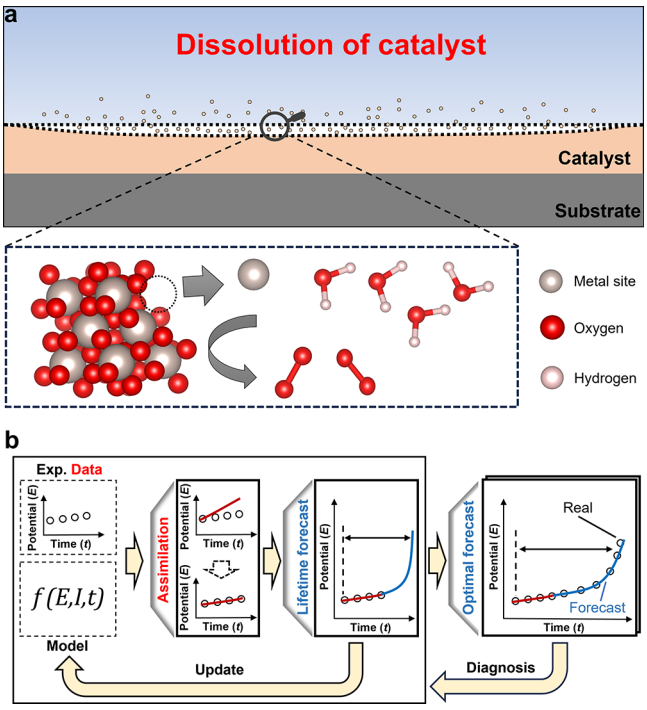

Figure 1. Schematic diagram. (a) OER electrocatalyst degradation mechanism in an aqueous system. Here the dissolution of solid catalyst is considered as the main driving force of degradation. (b) Integration of experimental data and theoretical model through DA to forecast the anode lifetime in an assimilation−forecasting−diagnosis cycle: model parameters are regulated based on present experimental information and the lifetime is forecasted, followed by refreshing experimental data and updating the model parameters through new assimilation toward improved forecasting; finally, highly accurate lifetime forecasting is achieved, with subsequent model diagnosis for further modification.

OER (please refer to part 1 in the SI for details of the degradation model):

$$E_{app} = \frac{1}{\alpha}\ln\frac{I-c}{k_0 S(t)} + I(R_0 + r_{RWE,1}t) \quad (1)$$

$$S(t) = \left(\left(k't + \frac{S_{max}^{\,1-x'}}{-1+x'}\right)(-1+x')\right)^{1/(1-x')} \quad (2)$$

where E_{app} is the applied potential, α is the coefficient for the influence of potential on the intrinsic OER activity, I is the anode current, c is the current from the substrate (here termed substrate current), k_0 is the pre-exponential factor for OER, $S(t)$ is the active site number changing with time t, R_0 is the initial additional resistance (i.e., the resistance mainly by electrolyte and substrate), $r_{RWE,1}$ is the rate of resistance change due to substrate passivation, k' is the apparent dissolution coefficient (in this work termed dissolution factor), x' is the apparent reaction order for dissolution, and S_{max} is the initial number of active sites.

After formulating the OER electrocatalyst degradation via the degradation model, we accessed the reliability by experiments in a three-electrode configuration employing RuO_x as the model electrocatalysts (Figure S3 in the SI). RuO_x is widely accepted as a representative OER electrocatalyst due to its distinguished activity toward OER,[45] and therefore, it has been commonly employed in academia and

https://doi.org/10.1021/acsenergylett.4c02868
ACS Energy Lett. 2025, 10, 22−29

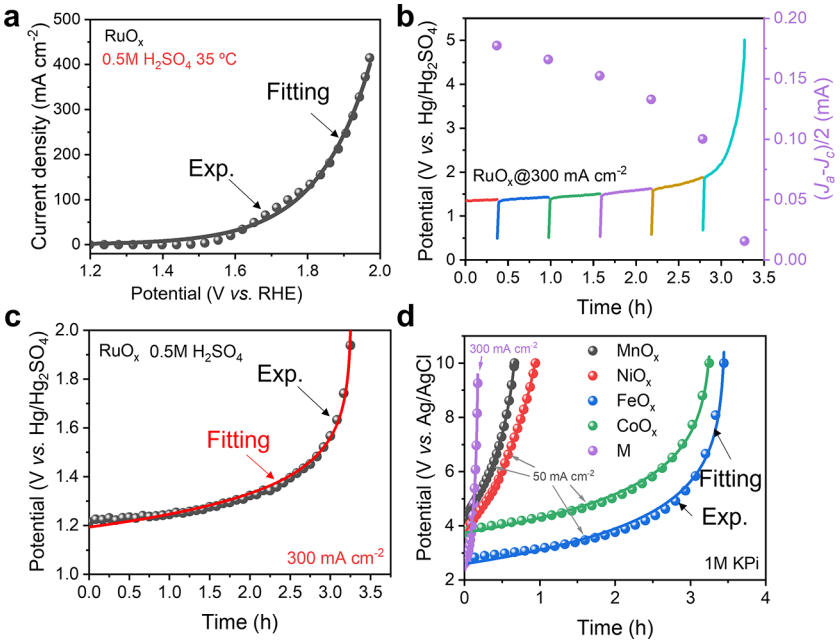

Figure 2. Verification of the degradation model. (a) Fitting of the polarization curve (1 mV s^{-1}) of the OER by eq 3; electrolyte: 0.5 M H_2SO_4 at 35 °C. (b) The trend of active site number during the OER durability testing; lines: chronopotentiometry curve with the current density fixed at 300 mA cm^{-2}, and downward lines were from continuing the measurement after pause; spheres: double-layer charging currents at 0.35 V (vs. Hg/Hg_2SO_4) with a scan rate of 100 mV s^{-1} after pausing the chronopotentiometry; electrolyte: 0.5 M H_2SO_4 at 35 °C. (c) Fitting of the OER degradation curve (current density fixed at 300 mA cm^{-2}) by the degradation model in 0.5 M H_2SO_4 at 35 °C and (d) application of the degradation model to other metal oxides (MnO_x, NiO_x, FeO_x, CoO_x) and a multicomponent material (including Mn, Ni, Fe, Zn, and Ag species, here noted as M) in 1 M KPi (pH 7) at 35 °C.

industry since the 1960s as the benchmark/model electrocatalyst in many studies in a wide pH range.[46−48] In our work, we focus on the dissolution process of electrocatalysts upon OER because the dissolution of metallic species is well-known as the main and common driving force of the intrinsic instability of metal-oxide-based electrocatalysts.[17,25,49,50] From this viewpoint, RuO_x is a particularly highly suitable material for our proof-of-concept to quantify the degradation process of OER as the dissolution mechanism of RuO_x during OER, i.e., soluble Ru-species formation under anodic OER conditions,[51] is well investigated due to the aforementioned features of this material. Therefore, herein, we chose RuO_x as the model OER electrocatalyst to make a model study. A polarization curve was first collected by using RuO_x as the electrocatalyst supported on a Ti substrate for the OER (see more about the synthesis in Experimental Methods), showing a typical "exponential" relationship between the current of the OER and the potential (Figure 2a). To match the current−potential polarization, we rewrote eq 1 by ignoring the substrate current (which was pretty small as compared with the current from RuO_x; see more discussion in Figure S4 in the SI) and setting t as 0, leading to the Butler−Volmer framework:[52]

$$I = I_0 e^{\alpha_0 F(E-E_0)/RT} \tag{3}$$

where I_0 is the exchange current density, α_0 is the transfer coefficient, F is Faradaic efficiency, E_0 is the equilibrium potential for OER, R is gas constant, and T is the temperature. As a result, it fit well the experimental results (Figure 2a), further indicated by the close-to-unity adjusted R-square (Table S1 in the SI). As shown in the degradation model, it suggested a strong correlation between the degradation and the change of the time-dependent active site number ($S(t)$). To solidify this relationship, we used chronopotentiometry to evaluate the electrocatalyst degradation. It was evident that with the increase of applied potential (i.e., the degradation of the OER electrocatalyst), the active site number was decreased, as indicated by the trend of double-layer charging current in Figure 2b (see more details in Figure S5 in the SI).

Following the above results, we applied the model to the degradation of the OER electrocatalyst monitored by chronopotentiometry. It showed almost overlapped plots of the measured and the fitted curves, further proved by the close-to-unity adjusted R-square (Figure 2c, Table S2 in the SI). The degradation model suggested a negative logarithmic relationship between the applied potential and the active site number; thus, experimentally there was gradual increase of the applied potential initially (e.g., until 2 h in Figure 2c) and a subsequent fast growth (e.g., after 2 h in Figure 2c), accompanied by the continuous reduction of active site number. Further results showed that our degradation model could not only be applied to acid but also neutral and alkaline conditions (Figure S6 and Tables S3 and S4 in the SI), various electrolyte concentrations (Figure S8 and Tables S11 and S12 in the SI), as well as higher temperatures (Figures S7 and S8c and Tables S5 and S13 in the SI) and different current densities (Figure S9 and Tables S14−S16 in the SI). As for the electrocatalysts, apart from the benchmark RuO_x, the degradation of other transition-metal-based materials, such as MnO_x, NiO_x, FeO_x, CoO_x, and M (a multicomponent electrocatalyst including Mn, Ni, Fe, Zn, and Ag, see the synthesis in Experimental Methods), could be well quantified through our model (Figure 2d, Tables S6−S10 in the SI).

All in all, the satisfying consistency between theoretical description and experimental data for the OER activity and durability testing revealed the high reliability of our degradation model. This result was also consistent with the

https://doi.org/10.1021/acsenergylett.4c02868
ACS Energy Lett. 2025, 10, 22−29

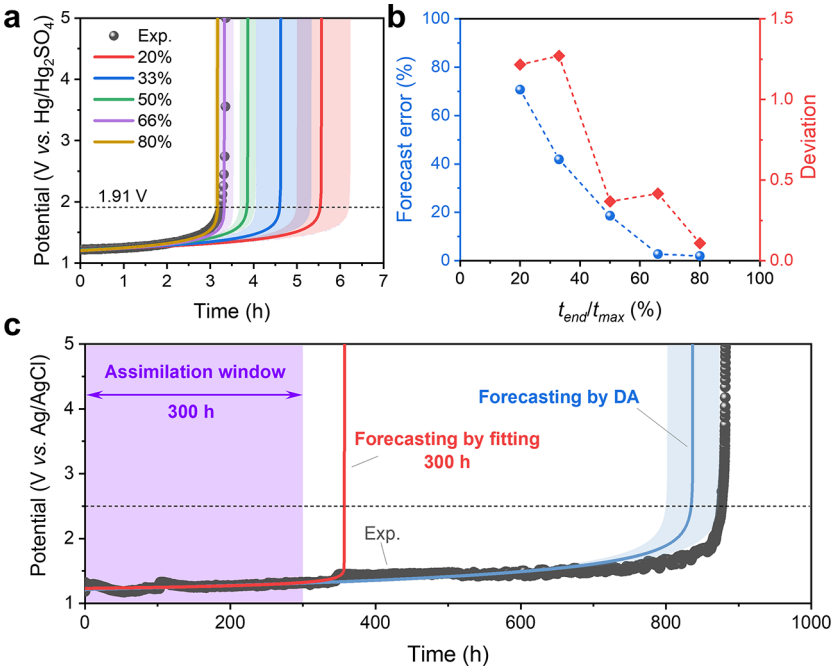

Figure 3. DAs for the OER electrocatalyst degradation. (a) Dynamically forecasting the lifetime of the OER anode with various assimilation windows (from 20% to 80% of the whole experimental period); experimental conditions: 0.5 M H_2SO_4 at 35 °C under 300 mA cm^{-2}, with RuO_x as the electrocatalyst for the OER. (b) Trend of the forecast error (spheres in the plots: the forecasted lifetime vs. the experimental lifetime; see more in eq 10 in Experimental Methods) with various assimilation windows from 20% to 80% of the whole measurement period (noted as t_{end}/t_{max}, in which t_{end} is the length of assimilation window and t_{max} is the whole period of experiment), and deviations of the forecasted lifetime (rhombuses in the plots). (c) Lifetime forecasting for long-term durability by DA with 34% of the whole data as well as the forecasting based on simple fitting by using the same data length; experimental conditions: 0.1 M sodium carbonate (pH 9.2) at 80 °C under 100 mA cm^{-2}, with RuO_x as the electrocatalyst for the OER.

previous reports about the depletion of electrocatalysts during durability testing.[26,53]

After successfully displaying the versatile application of our model in OER electrocatalyst degradation under various conditions, we combined a data science-based approach, i.e., the DA, to carry out dynamic lifetime forecasting to shorten the time frame for degradation evaluation (see more details in Experimental Methods). The experimental data (spheres in Figure 3a) could be roughly divided into two parts: the slow and ultrarapid increases of applied potential. Transition from the slow to the ultrarapid indicated a process from sluggish degradation to collapse. For convenience, we empirically set the time at 1.91 V (vs. Hg/Hg_2SO_4), featuring steep changes of applied potentials, as the anode lifetimes for the results are shown in Figure 3a. It was evident that as the length of assimilation window increased from 20% to 80% of the whole period, the forecasted lifetime decreased from 5.54 to 3.18 h, approaching the experimental 3.24 h. A further comparison was conducted by monitoring the trend of the forecast error (the forecasted lifetime vs. the experimental lifetime; see more details in eq 10 in Experimental Methods). The decrease in this forecast error from 71% to 2% clearly exhibited an improving forecast ability with updating the degradation data (spheres in Figure 3b). This was further verified by the reducing trend of deviation for the forecasted lifetime (rhombuses in Figure 3b). We further carried out DAs for degradation processes with other lifetimes to show the capability of our DA-based method (Figure S10 in the SI). Next, we carried out a model diagnosis (see the details in Figure S11 in the SI). We found that even under the simplification the degradation model still worked well, and the dissolution factor (k') was crucial to achieving accurate lifetime forecasting.

To demonstrate the practical applicability of DA, by using a short assimilation window (34% of the whole period, i.e., 300 h), the lifetime (at 2.5 V) was accurately forecasted with a small error of 4% for the nearly 1000 h durability testing (Figure 3c). For further highlighting the DA in lifetime forecasting, we carried out simple fittings by using various data lengths for comparison (Figure 3c; Figure S14 and Tables S18−S23 in the SI; see also Experimental Methods). In the case of using experimental data up to 300 h, the prediction error by simple fitting was much larger (60%, Figure S15 in the SI) than that of DA (4%). Moreover, the fitting approach required experimental data up to approximately the same time as the lifetime to forecast as accurately as the DA (Figure S15 in the SI). Such superior forecast ability by DA to simple fitting demonstrated better parameter optimization of DA. This could be attributed to the Bayesian inference in DA, making it skilled at optimizing model parameters for reliable lifetime forecasting especially with nonuniform uncertainties (as indicated by the fluctuations of the experimental data in Figure 3c). In addition, even though it is known that several modern computation-based approaches, typically molecular dynamics simulation or machine learning, enable determining model parameters, these methods still suffer from the limitation of short time scale or high cost of preparing massive training data sets.[54,55] Therefore, our approach employing DA is more promising and practically useful than the existing typical approaches in forecasting the anode lifetime with optimized model parameters by the OER degradation model (see a detailed discussion on pages 26 and 27 and Figure S13 in the SI).

https://doi.org/10.1021/acsenergylett.4c02868
ACS Energy Lett. 2025, 10, 22−29

Our method is based on a mechanism with a single degradation driving force, i.e., the dissolution-driven degradation, leading to some limitations such as the difficulty in treating degradation by other mechanisms (see further discussions on the limitations of our method on page 26 and in Figure S16 in the SI). Nonetheless, our knowledge-contained model enables satisfying interpretability for the matched anode degradation process (see a detailed discussion in Figure S17 in the SI). In addition, given a comprehensive degradation model including multiple degradation processes, it is possible to clarify the dominant degradation mechanism based on the DA method proposed in this study. For example, after determining all the parameters at a time t in a model by DA, we can analyze the partial derivative of the model with respect to t for each degradation mechanism. As a result, we will obtain a quantitative evaluation of the influence of each degradation mechanism on the overall degradation behavior. By comparing the above results, we can finally confirm that the maximum absolute partial derivative (and much larger than others) corresponds to the dominant degradation mechanism. Moreover, this method can identify a dynamic dominant degradation mechanism that evolves with the degradation process because of the inclusion of time. Based on the above consideration and inspired by *control function* (or *control factor*) and *degree of rate control* for quantifying the rate-determining step in chemical kinetics,[56,57] herein we propose *degree of degradation control*, *i.e.*, $r_{d,i}(t)$, to quantify the influence of degradation mechanisms on stability:

$$r_{d,i}(t) = \frac{R_{d,i}(t)}{\sum_i |R_{d,i}(t)|} \tag{4}$$

where $R_{d,i}(t)$ is the influence on the overall degradation by the ith degradation mechanism at time t. We may also extend this concept to not only degradation but also upgradation (i.e., the promotion of electrode performance), which are further unified by the term "destabilization" so that *degree of destabilization control* can be nominated. For a detailed discussion, including a complete mathematical description, please refer to part 3 and eqs S33−S35 in the SI.

In summary, we conducted a quantification of OER electrocatalyst degradation with a data-driven approach. Based on the energetic-span kinetic framework, we established an effective electrocatalyst degradation model for the OER, which was further verified by experimental results with various conditions and electrocatalysts. The subsequent application of this degradation model was iteratively implemented by using a DA method, achieving dynamic lifetime forecasting through continuous updating of degradation data. This approach led to robust and accurate multidimensional parameter optimization, with clear advantages over existing computational methods, as evidenced by quantitative comparison. We launched a model diagnosis based on DA to track the key parameters. This diagnosis indicated that even though the degradation model simplified both the kinetics of the OER and the process of active site loss, it was still accessible to reliable lifetime forecasting based on the DA method. We believe that the closed-loop study of this work by a data-driven approach, including theory establishment and verification, application, and model diagnosis, will benefit the understanding of OER electrocatalyst degradation and accelerate the rational development of highly efficient electrodes, especially with long-term stabilities, for electrochemistry-based technologies in the crucial next few decades to achieve carbon neutrality.

EXPERIMENTAL METHODS

Chemicals. $RuCl_3{\cdot}xH_2O$ (Ru > 40%) was purchased from Tokyo Chemical Industry Co., Ltd. $MnCl_2{\cdot}4H_2O$ (99.0%), $NiCl_2{\cdot}6H_2O$ (98.0%), $FeCl_2{\cdot}4H_2O$ (99.0%), $AgNO_3$ (99.8%), KH_2PO_4 (>99.5%), KOH (>85%), and ethanol (99.5%) were from Wako Fuji Co. Ltd. $ZnCl_2$ (99.95%) was purchased from Alfa Aesar. $CoCl_2$ $6H_2O$ (99.0%) was purchased from Hayashi Pure Chemical Ind., Ltd. H_2SO_4 (96.0%) was from KANTO CHEMICAL CO.,INC. Ultrapure water (18.2 MΩ·cm, Milli-Q IQ Element, Merck AG, Germany) was used to prepare electrolytes.

Pretreatment of Ti foil. The titanium (Ti) foil (Ti, 99.5%, Nilaco, 0.05 × 5 × 30 mm) was cleaned by ethanol and ultrapure water and subsequently etched in an oxalic acid solution (10%) at 80 °C for 1 h. Finally, the Ti foil was rinsed by ultrapure water and dried in air.

Synthesis of RuO_x. A precursor solution (0.05 M $RuCl_3$ in ethanol) was dropped (2.5 μL) on the pretreated Ti substrate (dropped region 5 × 10 mm) and subsequently annealed at 350 °C for 10 min in air. The above process was repeated another nine times and finally annealed at 460 °C for 70 min in air.

Synthesis of MO_x (M = Mn, Ni, Fe, Co). Similar methods were used for the synthesis of RuO_x, apart from that the precursor was replaced by $MnCl_2$, $NiCl_2$, $FeCl_2$, and $CoCl_2$, respectively.

Synthesis of Multicomponent Oxide (M). A silver precursor solution (0.05 M $AgNO_3$ in ethanol) was dropped (0.5 μL) on the pretreated Ti substrate, followed by dropping a mixture (2.0 μL, totally 0.05 M metal species in ethanol by mixing $MnCl_2$, $NiCl_2$, $FeCl_2$, and $ZnCl_2$) of a molar ratio of 1:1:1:0.5 for Mn:Ni:Fe:Zn. After being dried, it was annealed at 350 °C for 10 min in air.[58] The above process was repeated another nine times, with final annealing at 460 °C for 70 min in air. The obtained catalyst on the Ti substrate was marked as M. The detailed method can be found in the reference.

Electrochemical Measurements. A three-electrode configuration in a water bath at 35 °C was used, with electrocatalysts on the pretreated Ti substrate as the working electrode; Pt coil as the counter electrode; and Hg/Hg_2SO_4 (saturated K_2SO_4), Ag/AgCl (3 M NaCl), and Hg/HgO (1 M KOH) as the reference electrode for acid, neutral, and alkali electrolyte, respectively (see more details in Figure S3 in the SI). Linear sweep voltammetry (LSV) was carried out with a scan rate of 1 mV s^{-1} if not specified. A chronopotentiometry (CP) method was conducted at fixed current densities for the evaluation of the degradation processes.

In the long-term stability testing, 0.1 M sodium carbonate (pH 9.2) was used as the electrolyte at 80 °C in a heating mantle, with RuO_x as the electrocatalyst on a pretreated Ti substrate for the OER, a Pt coil as the counter electrode, and Ag/AgCl (3 M KCl) as the reference electrode. A chronopotentiometry (CP) method was conducted to access the degradation process after the aging period.

Double-layer charging currents were used to monitor the trend of active site number during the degradation process by a cyclic voltammetry (CV) method. The CV tests were carried out with a scan rate of 100 mV s^{-1} in 0.30−0.40 V (vs. Hg/Hg_2SO_4) after the CP measurement. The half of the difference between the current in the anodic scan (J_a) and the current in

https://doi.org/10.1021/acsenergylett.4c02868
ACS Energy Lett. 2025, 10, 22−29

the cathodic scan (J_c) at 0.35 V (vs. Hg/Hg_2SO_4) served as the typical double-layer charging currents.

Data Assimilation (DA). A nonsequential data assimilation method minimizing the cost function using tree-structured Parzen estimator (DMC-TPE), was used for the OER degradation process in this work.[28] For the DAs, at time t a state vector $\mathbf{x}_t$ ($0 < t \leq t_{end}$, where t_{end} represents the length of the assimilation window) was defined, including the applied potential and its first-order derivative with respect to time. The $\mathbf{x}_t$ is expressed as

$$\mathbf{x}_t = \left[E_{app}|_t, \left.\frac{dE_{app}}{dt}\right|_t \right]^T \tag{5}$$

where the superscript T represents for the transposition. In this study, $\mathbf{x}_t$ could be calculated as

$$\mathbf{x}_t = M(\mathbf{x}_0, t) \tag{6}$$

where M indicates the degradation model and $\mathbf{x}_0$ is a vector consisting of the parameters of the model to be estimated.

Moreover, at time t we defined the observation vector $\mathbf{y}_t$, which contained the experimentally collected applied potential and its first-order derivatives with time. Notably, both $\mathbf{x}_t$ and $\mathbf{y}_t$ were treated as stochastic variables in DA. The cost function $J(\mathbf{x}_0)$ to evaluate the misfit between $\mathbf{x}_t$ and $\mathbf{y}_t$ was expressed as

$$J(\mathbf{x}_0) = \frac{1}{2}(\mathbf{x}_0 - \mathbf{x}_0^b)^T \mathbf{B}^{-1}(\mathbf{x}_0 - \mathbf{x}_0^b) + \sum_t^{t_{end}} \frac{1}{2}(M(\mathbf{x}_0, t) - y_t)^T \mathbf{R}_t^{-1}(M(\mathbf{x}_0, t) - \mathbf{y}_t) \tag{7}$$

in which $\mathbf{x}_0^b$ is the background vector. $\mathbf{B}$ and $\mathbf{R}_t$ are the covariance matrices of the background and observation errors, respectively. When the optimal vector $\mathbf{x}_0^a$ that minimizes $J(\mathbf{x}_0)$ was obtained, the corresponding state vector $\mathbf{x}_t = M(\mathbf{x}_0^a, t)$ was regarded as the optimal forecast. The coefficients in the degradation model a, k_0, and k' were estimated in the DAs. The parameter x' was fixed as 0.01 to release the parameter k' during the DAs. In this study, we conducted five DAs in which the length of the assimilation window t_{end} was varied in ratios of 20%, 33%, 50%, 66%, and 80% as compared with the whole period of the experiment, t_{max}. Because the DMC-TPE method depends on random numbers, the estimated parameters for each t_{end} were evaluated with the mean and standard deviation (SD) obtained from five results of DA using different random seed. In the DA for $t_{end} = 0.2t_{max}$, the first term of eq 7 was neglected because of the difficulty in determining $\mathbf{x}_0^b$ and $\mathbf{B}$. In all other DAs, $\mathbf{x}_0^b$ and $\mathbf{B}$ were determined based on the means and SDs of one previous DA result: $\mathbf{x}_0^b = [m_a, m_{k0}, m_{k'}]^T$ and $\mathbf{B} = \mathrm{diag}[\sigma_a, \sigma_{k0}, \sigma_k]$. Note that in our DAs, $\mathbf{x}_0^b$ and $\mathbf{B}$ would not significantly affect the estimation results because the first term of $J(\mathbf{x}_0)$ is sufficiently small compared to the second term. $\mathbf{R}_t$ was defined as $\mathbf{R}_t = [\sigma_t^2, \sigma_t'^2]$, where σ_t and σ_t' denote parameters which determine the magnitude of the observational noises in E_{app} and dE_{app}/dt, respectively. By assuming that the more recent data more strongly reflect an increase in E_{app}, σ_t and σ_t' are defined as follows:

$$\sigma_t = 0.0002(t_{end} - t) + 0.0001 \tag{8}$$

$$\sigma_t' = 0.01(t_{end} - t) + 0.005 \tag{9}$$

The forecast error (%) was calculated by

$$\text{forecast error} = \left| \frac{\text{forecasted lifetime} - \text{experimental lifetime}}{\text{experimental lifetime}} \right| \times 100 \tag{10}$$

For the long-term durability testing, to diminish detrimental effects from noises, σ_t and σ_t' are defined as follows:

$$(\sigma_t, \sigma_t') = \begin{cases} (0.001, 0.05), \text{ if } t < 150 \text{ or } 340 \leq t < 360 \\ (0.0001, 0.005), \text{ otherwise} \end{cases} \tag{11}$$

Furthermore, before DA was conducted, preprocessing was implemented by smoothing the data from the beginning to 400 h. The period until 300 h served as the assimilation window.

Lifetime Forecasting by Simple Fitting. The developed degradation model in this work was used to fit the collected degradation data (i.e., the potential-time result), with a tolerance value of 10^{-9}. The anode lifetime was then forecasted by using the degradation model with the fitted model parameters.

Computational Requirements. The computational cost of DA using the degradation model is low. DA is able to be conducted on an ordinary desktop or laptop personal computer without a workstation dedicated to numerical calculations. We conducted the DAs using a central process unit (CPU, Intel Core i9-11900 2.50 GHz), and one DA step took approximately 15 min. Therefore, it will be possible for our DA-based approach to exhibit large scalability with low-cost computations.

■ ASSOCIATED CONTENT

Supporting Information

The Supporting Information is available free of charge at https://pubs.acs.org/doi/10.1021/acsenergylett.4c02868.

Additional kinetic analysis, experimental configuration, polarization curves, fitting results, CV plots, data assimilations, machine learning results, and discussions on limitations of our method (PDF)

■ AUTHOR INFORMATION

Corresponding Author

Ken Sakaushi − *Research Center for Energy and Environmental Materials, National Institute for Materials Science, Tsukuba, Ibaraki 305-0044, Japan;* orcid.org/0000-0003-4797-9087; Email: SAKAUSHI.Ken@nims.go.jp

Authors

Miao Wang − *Research Center for Energy and Environmental Materials, National Institute for Materials Science, Tsukuba, Ibaraki 305-0044, Japan*

Akimitsu Ishii − *International Center for Young Scientists, National Institute for Materials Science, Tsukuba, Ibaraki 305-0047, Japan*

Complete contact information is available at: https://pubs.acs.org/10.1021/acsenergylett.4c02868

Author Contributions

K.S. conceived the idea and coordinated and supervised this project. K.S. and M.W. designed the experiments and analytical methods together with A.I. M.W. carried out the experiments

https://doi.org/10.1021/acsenergylett.4c02868
ACS Energy Lett. 2025, 10, 22−29

and A.I. data assimilation. M.W. wrote the initial draft, and K.S. and A.I. cowrote the paper. All the authors have given approval for the final version of the manuscript.

Notes

The authors declare the following competing financial interest(s): K.S., M.W., and A.I. have filed a patent (application number JP2024-97657).

■ ACKNOWLEDGMENTS

This work was supported by the MEXT Program: Data Creation and Utilization-Type Material Research and Development Project Grant Number JPMXP1122712807. The authors are indebted to the National Institute for Material Science. We thank Dr. Wenqin Peng for conducting the long-term durability test and providing us the data.

■ REFERENCES

(1) Hydrogen Council; McKinsey & Company. Hydrogen Insights 2023. 2023.

(2) Hoisang, W.; Sakaushi, K. Key criteria for next-generation dimensionally stable electrodes towards large-scale green hydrogen production by water electrolysis. *Current Opinion in Electrochemistry* **2022**, *36*, 101136.

(3) Nicholson, W.; Carlisle, S. A.; Cruickshank, W., IV Experiments in galvanic electricity. *Philosophical Magazine* **1800**, *7* (28), 337−347.

(4) Seh, Z. W.; Kibsgaard, J.; Dickens, C. F.; Chorkendorff, I.; Nørskov, J. K.; Jaramillo, T. F. Combining theory and experiment in electrocatalysis: Insights into materials design. *Science* **2017**, *355* (6321), No. eaad4998.

(5) Chatenet, M.; Pollet, B. G.; Dekel, D. R.; Dionigi, F.; Deseure, J.; Millet, P.; Braatz, R. D.; Bazant, M. Z.; Eikerling, M.; Staffell, I.; et al. Water electrolysis: from textbook knowledge to the latest scientific strategies and industrial developments. *Chem. Soc. Rev.* **2022**, *51* (11), 4583−4762.

(6) Hori, Y.; Kikuchi, K.; Suzuki, S. Production of CO and CH_4 in electrochemical reduction of CO_2 at metal electrodes in aqueous hydrogencarbonate solution. *Chem. Lett.* **1985**, *14* (11), 1695−1698.

(7) García de Arquer, F. P.; Dinh, C.-T.; Ozden, A.; Wicks, J.; McCallum, C.; Kirmani, A. R.; Nam, D.-H.; Gabardo, C.; Seifitokaldani, A.; Wang, X.; et al. CO_2 electrolysis to multicarbon products at activities greater than 1 A cm^{-2}. *Science* **2020**, *367* (6478), 661−666.

(8) Furuya, N.; Yoshiba, H. Electroreduction of nitrogen to ammonia on gas-diffusion electrodes loaded with inorganic catalyst. *Journal of Electroanalytical Chemistry and Interfacial Electrochemistry* **1990**, *291* (1), 269−272.

(9) Tsuneto, A.; Kudo, A.; Sakata, T. Efficient Electrochemical Reduction of N2 to NH3 Catalyzed by Lithium. *Chem. Lett.* **1993**, *22* (5), 851−854.

(10) Zhou, F.; Azofra, L. M.; Ali, M.; Kar, M.; Simonov, A. N.; McDonnell-Worth, C.; Sun, C.; Zhang, X.; MacFarlane, D. R. Electro-synthesis of ammonia from nitrogen at ambient temperature and pressure in ionic liquids. *Energy Environ. Sci.* **2017**, *10* (12), 2516−2520.

(11) Li, S.; Zhou, Y.; Fu, X.; Pedersen, J. B.; Saccoccio, M.; Andersen, S. Z.; Enemark-Rasmussen, K.; Kempen, P. J.; Damsgaard, C. D.; Xu, A.; et al. Long-term continuous ammonia electrosynthesis. *Nature* **2024**, *629* (8010), 92−97.

(12) Kanan, M. W.; Nocera, D. G. In Situ Formation of an Oxygen-Evolving Catalyst in Neutral Water Containing Phosphate and Co^{2+}. *Science* **2008**, *321* (5892), 1072−1075.

(13) Xiao, L.; Zhang, S.; Pan, J.; Yang, C.; He, M.; Zhuang, L.; Lu, J. First implementation of alkaline polymer electrolyte water electrolysis working only with pure water. *Energy Environ. Sci.* **2012**, *5* (7), 7869−7871.

(14) Li, A.; Kong, S.; Adachi, K.; Ooka, H.; Fushimi, K.; Jiang, Q.; Ofuchi, H.; Hamamoto, S.; Oura, M.; Higashi, K.; et al. Atomically dispersed hexavalent iridium oxide from MnO_2 reduction for oxygen evolution catalysis. *Science* **2024**, *384* (6696), 666−670.

(15) Nuttall, L. J.; Fickett, A. P.; Titterington, W. A. Hydrogen Generation by Solid Polymer Electrolyte Water Electrolysis. In *Hydrogen Energy: Part A*; Veziroğlu, T. N., Ed.; Springer: US, 1975; pp 441−455.

(16) Ouimet, R. J.; Glenn, J. R.; De Porcellinis, D.; Motz, A. R.; Carmo, M.; Ayers, K. E. The Role of Electrocatalysts in the Development of Gigawatt-Scale PEM Electrolyzers. *ACS Catal.* **2022**, *12* (10), 6159−6171.

(17) Danilovic, N.; Subbaraman, R.; Chang, K.-C.; Chang, S. H.; Kang, Y. J.; Snyder, J.; Paulikas, A. P.; Strmcnik, D.; Kim, Y.-T.; Myers, D.; et al. Activity-Stability Trends for the Oxygen Evolution Reaction on Monometallic Oxides in Acidic Environments. *J. Phys. Chem. Lett.* **2014**, *5* (14), 2474−2478.

(18) Geiger, S.; Kasian, O.; Mingers, A. M.; Nicley, S. S.; Haenen, K.; Mayrhofer, K. J. J.; Cherevko, S. Catalyst Stability Benchmarking for the Oxygen Evolution Reaction: The Importance of Backing Electrode Material and Dissolution in Accelerated Aging Studies. *ChemSusChem* **2017**, *10* (21), 4140−4143.

(19) Geiger, S.; Kasian, O.; Ledendecker, M.; Pizzutilo, E.; Mingers, A. M.; Fu, W. T.; Diaz-Morales, O.; Li, Z.; Oellers, T.; Fruchter, L.; et al. The stability number as a metric for electrocatalyst stability benchmarking. *Nature Catalysis* **2018**, *1* (7), 508−515.

(20) Fabbri, E.; Schmidt, T. J. Oxygen Evolution Reaction—The Enigma in Water Electrolysis. *ACS Catal.* **2018**, *8* (10), 9765−9774.

(21) Grimaud, A.; Diaz-Morales, O.; Han, B.; Hong, W. T.; Lee, Y.-L.; Giordano, L.; Stoerzinger, K. A.; Koper, M. T. M.; Shao-Horn, Y. Activating lattice oxygen redox reactions in metal oxides to catalyse oxygen evolution. *Nat. Chem.* **2017**, *9* (5), 457−465.

(22) Sakaushi, K.; Kumeda, T.; Hammes-Schiffer, S.; Melander, M. M.; Sugino, O. Advances and challenges for experiment and theory for multi-electron multi-proton transfer at electrified solid-liquid interfaces. *Phys. Chem. Chem. Phys.* **2020**, *22* (35), 19401−19442.

(23) Sakaushi, K.; Uosaki, K. Computationally empowered design of emerging earth-abundant electrocatalysts toward electron- /proton-transferring energy conversion. *Current Opinion in Electrochemistry* **2021**, *26*, 100661.

(24) Topalov, A. A.; Katsounaros, I.; Auinger, M.; Cherevko, S.; Meier, J. C.; Klemm, S. O.; Mayrhofer, K. J. J. Dissolution of Platinum: Limits for the Deployment of Electrochemical Energy Conversion? *Angew. Chem., Int. Ed.* **2012**, *51* (50), 12613−12615.

(25) Cherevko, S.; Zeradjanin, A. R.; Topalov, A. A.; Kulyk, N.; Katsounaros, I.; Mayrhofer, K. J. J. Dissolution of Noble Metals during Oxygen Evolution in Acidic Media. *ChemCatChem.* **2014**, *6* (8), 2219−2223.

(26) Wang, Q.; Cheng, Y.; Tao, H. B.; Liu, Y.; Ma, X.; Li, D.-S.; Yang, H. B.; Liu, B. Long-Term Stability Challenges and Opportunities in Acidic Oxygen Evolution Electrocatalysis. *Angew. Chem., Int. Ed.* **2023**, *62* (11), No. e202216645.

(27) Ishii, A.; Yamanaka, A.; Miyoshi, E.; Okada, Y.; Yamamoto, A. Estimation of solid-state sintering and material parameters using phase-field modeling and ensemble four-dimensional variational method. *Modell. Simul. Mater. Sci. Eng.* **2021**, *29* (6), 065012.

(28) Ishii, A.; Yamamoto, A.; Yamanaka, A. DMC-TPE: tree-structured Parzen estimator-based efficient data assimilation method for phase-field simulation of solid-state sintering. *Science and Technology of Advanced Materials: Methods* **2023**, *3* (1), 2239133.

(29) Ghil, M.; Malanotte-Rizzoli, P. Data Assimilation in Meteorology and Oceanography. In *Advances in Geophysics*; Dmowska, R., Saltzman, B., Eds.; Vol. *33*; Elsevier, 1991; pp 141−266.

(30) Simon, E.; Bertino, L. Application of the Gaussian anamorphosis to assimilation in a 3-D coupled physical-ecosystem model of the North Atlantic with the EnKF: a twin experiment. *Ocean Sci.* **2009**, *5* (4), 495−510.

(31) Lewis, J. M. Sasaki's Pathway to Deterministic Data Assimilation. In *Data Assimilation for Atmospheric, Oceanic and*

https://doi.org/10.1021/acsenergylett.4c02868
ACS Energy Lett. 2025, 10, 22−29

Hydrologic Applications; Park, S. K., Xu, L., Eds.; Springer: Berlin, 2009; pp 1−19.
(32) Sakaushi, K.; Watanabe, A.; Kumeda, T.; Shibuta, Y. Fast-Decoding Algorithm for Electrode Processes at Electrified Interfaces by Mean-Field Kinetic Model and Bayesian Data Assimilation: An Active-Data-Mining Approach for the Efficient Search and Discovery of Electrocatalysts. *ACS Appl. Mater. Interfaces* **2022**, *14* (20), 22889−22902.
(33) Sakaushi, K.; Shibuta, Y. Data-Assimilation-Based Algorithm to Unveil Electrode Processes. *Denki Kagaku* **2023**, *91* (2), 169−177.
(34) Rudin, C. Stop explaining black box machine learning models for high stakes decisions and use interpretable models instead. *Nature Machine Intelligence* **2019**, *1* (5), 206−215.
(35) Amatore, C.; Jutand, A. Mechanistic and kinetic studies of palladium catalytic systems. *J. Organomet. Chem.* **1999**, *576* (1), 254−278.
(36) Kozuch, S.; Shaik, S. A Combined Kinetic-Quantum Mechanical Model for Assessment of Catalytic Cycles: Application to Cross-Coupling and Heck Reactions. *J. Am. Chem. Soc.* **2006**, *128* (10), 3355−3365.
(37) Kozuch, S.; Shaik, S. Kinetic-Quantum Chemical Model for Catalytic Cycles: The Haber-Bosch Process and the Effect of Reagent Concentration. *J. Phys. Chem. A* **2008**, *112* (26), 6032−6041.
(38) Kozuch, S.; Shaik, S. How to Conceptualize Catalytic Cycles? The Energetic Span Model. *Acc. Chem. Res.* **2011**, *44* (2), 101−110.
(39) Chen, J.; Chen, Y.; Li, P.; Wen, Z.; Chen, S. Energetic Span as a Rate-Determining Term for Electrocatalytic Volcanos. *ACS Catal.* **2018**, *8* (11), 10590−10598.
(40) Wang, M.; Kong, H.; Wang, J. Revisiting electrocatalytic oxygen evolution reaction microkinetics from a mathematical viewpoint. *Results in Chemistry* **2023**, *5*, 100985.
(41) Chen, F.-Y.; Wu, Z.-Y.; Adler, Z.; Wang, H. Stability challenges of electrocatalytic oxygen evolution reaction: From mechanistic understanding to reactor design. *Joule* **2021**, *5* (7), 1704−1731.
(42) Risch, M. Upgrading the detection of electrocatalyst degradation during the oxygen evolution reaction. *Current Opinion in Electrochemistry* **2023**, *38*, 101247.
(43) Binninger, T.; Mohamed, R.; Waltar, K.; Fabbri, E.; Levecque, P.; Kötz, R.; Schmidt, T. J. Thermodynamic explanation of the universal correlation between oxygen evolution activity and corrosion of oxide catalysts. *Sci. Rep.* **2015**, *5* (1), 12167.
(44) Cherevko, S. Stability and dissolution of electrocatalysts: Building the bridge between model and "real world" systems. *Current Opinion in Electrochemistry* **2018**, *8*, 118−125.
(45) Kibsgaard, J.; Chorkendorff, I. Considerations for the scaling-up of water splitting catalysts. *Nature Energy* **2019**, *4* (6), 430−433.
(46) De Nora, O. Anwendung maßbeständiger aktivierter Titan-Anoden bei der Chloralkali-Elektrolyse. *Chemie Ingenieur Technik* **1970**, *42* (4), 222−226.
(47) Trasatti, S. Electrocatalysis in the anodic evolution of oxygen and chlorine. *Electrochim. Acta* **1984**, *29* (11), 1503−1512.
(48) Trasatti, S. Electrocatalysis: understanding the success of DSA®. *Electrochim. Acta* **2000**, *45* (15), 2377−2385.
(49) Kasian, O.; Grote, J.-P.; Geiger, S.; Cherevko, S.; Mayrhofer, K. J. J. The Common Intermediates of Oxygen Evolution and Dissolution Reactions during Water Electrolysis on Iridium. *Angew. Chem., Int. Ed.* **2018**, *57* (9), 2488−2491.
(50) Ledendecker, M.; Mondschein, J. S.; Kasian, O.; Geiger, S.; Göhl, D.; Schalenbach, M.; Zeradjanin, A.; Cherevko, S.; Schaak, R. E.; Mayrhofer, K. Stability and Activity of Non-Noble-Metal-Based Catalysts Toward the Hydrogen Evolution Reaction. *Angew. Chem., Int. Ed.* **2017**, *56* (33), 9767−9771.
(51) Du, K.; Zhang, L.; Shan, J.; Guo, J.; Mao, J.; Yang, C.-C.; Wang, C.-H.; Hu, Z.; Ling, T. Interface engineering breaks both stability and activity limits of RuO_2 for sustainable water oxidation. *Nat. Commun.* **2022**, *13* (1), 5448.
(52) Inzelt, G. Milestones of the development of kinetics of electrode reactions. *J. Solid State Electrochem.* **2011**, *15* (7), 1373−1389.
(53) Kong, S.; Li, A.; Long, J.; Adachi, K.; Hashizume, D.; Jiang, Q.; Fushimi, K.; Ooka, H.; Xiao, J.; Nakamura, R. Acid-stable manganese oxides for proton exchange membrane water electrolysis. *Nature Catalysis* **2024**, *7* (3), 252−261.
(54) Zhao, W.; Ji, Y.; Zhang, Z.; Lin, M.; Wu, Z.; Zheng, X.; Li, Q.; Yang, Y. Recent advances in the research of functional electrolyte additives for lithium-ion batteries. *Current Opinion in Electrochemistry* **2017**, *6* (1), 84−91.
(55) Chen, H.; Kätelhön, E.; Compton, R. G. Machine learning in fundamental electrochemistry: Recent advances and future opportunities. *Current Opinion in Electrochemistry* **2023**, *38*, 101214.
(56) Laidler, K. J. Rate controlling step: A necessary or useful concept? *J. Chem. Educ.* **1988**, *65* (3), 250.
(57) Campbell, C. T. Future Directions and Industrial Perspectives Micro- and macro-kinetics: Their relationship in heterogeneous catalysis. *Top. Catal.* **1994**, *1* (3), 353−366.
(58) Sakaushi, K.; Hoisang, W.; Tamura, R. Human−Machine Collaboration for Accelerated Discovery of Promising Oxygen Evolution Electrocatalysts with On-Demand Elements. *ACS Central Science* **2023**, *9*, 2216−2224.

https://doi.org/10.1021/acsenergylett.4c02868
ACS Energy Lett. 2025, 10, 22−29